Received 12 May 2020; revised 17 June 2020; accepted 21 June 2020. Date of publication 25 June 2020; date of current version 20 July 2020.

Digital Object Identifier 10.1109/OJCOMS.2020.3004631

Performance Trade-Offs of an Optical Wireless Communication Network Deployed in an Aircraft Cockpit

STEVE JOUMESSI-DEMEFFO [1], STÉPHANIE SAHUGUÈDE [1], ANNE JULIEN-VERGONJANNE [1], AND PIERRE COMBEAU [2]

[1] XLIM Laboratory, UMR CNRS 7252, University of Limoges, 87000 Limoges, France

[2] XLIM Laboratory, UMR CNRS 7252, University of Poitiers, 86073 Poitiers, France

CORRESPONDING AUTHOR: A. JULIEN-VERGONJANNE (e-mail: anne.julien-vergonjanne@unilim.fr)

This work was funded by the European Union under Grant 737645, through the Cleansky2 H2020 project titled Aircraft Light Communication (ALC).

ABSTRACT In this article, we explore the performance of optical wireless technology for ensuring audio communications inside an aircraft cockpit. One advantage is that, unlike radio frequencies, opaque objects block optical signals and, therefore, signals cannot pass through walls. This can reduce security risks against eavesdropping and hacking of the physical layer, which is one of the main concerns in the aviation environment. However, optical wireless technology faces some issues, including range limitation and sensitivity to blockages. To study the achievable performances, we propose a modeling of the channels for the uplink and the downlink between the headsets of the four pilots of an Airbus A350 and the access point at the cockpit ceiling. A ray-tracing approach associated with a Monte-Carlo method takes into account the 3D geometric model of the cockpit, the presence of the pilots and their movements. We show that using spatial diversity for headset transceivers can improve performance. Using IEEE 802.11 medium access control mechanism to ensure multi-user communication, the approach highlights the trade-offs between power and delay for a successful communication, linked to the maximum achievable data rate for a given performance level.

INDEX TERMS Optical wireless communication, channel modeling, channel access control, in-flight communications.

I. INTRODUCTION

On CURRENT commercial airliners, communications between the aircraft and the devices used by the pilots in the cockpit, such as the headset, are based on wired or radiofrequency (RF) connections like Wi-Fi. A wireless connection is much more efficient and provides comfort and mobility to the pilots. Actually, wired headsets are well known to cause pain for long-haul flights, contributing to increased pilot stress, which can be critical especially for operations where the safety margin is already low (for example, take-off or landing). Wireless communication is also an opportunity to introduce new services and functionalities by taking advantage of the flexibility offered by mobile devices. Furthermore, the use of wireless technologies to replace aircraft cables can help reduce weight and therefore fuel consumption and CO2 emissions [1]. However, although effective, RF-based wireless solutions suffer from some drawbacks. Due to radio waves propagation nature, one problem is that the signal can be scrambled or listened to because RF waves can penetrate through walls, exposing the information conveyed by these signals to hackers [2]. In addition, RF communications are sensitive to electromagnetic interferences. These issues limit the RF use for such a sensitive environment as the cockpit where safety and security are paramount.

The use of optical technologies is one way to improve the security against eavesdropping at the physical layer because, unlike RF systems, opaque objects block the light and optical signals and, therefore, optical signals cannot pass through walls. Optical wireless communication (OWC) is thus a promising alternative approach [3]–[6], which has advantages in the studied scenario because there is no interference

This work is licensed under a Creative Commons Attribution 4.0 License. For more information, see https://creativecommons.org/licenses/by/4.0/

with or disruption of existing radio frequency connections. In addition, it is robust against hacking problems and can therefore offer a higher level of security than RF signals as used for example for Bluetooth headset. This emerging technology has been studied for in-flight applications and services relating to passengers in the cabin [7]–[11]. For example, the scenarios concerned entertainment [7], video broadcasting [8], communications between passengers [9], and even medical surveillance of travelers [10]. However, the advantage of confined communications can also constitute drawbacks because the range is limited and performance is very sensitive to blockages. Thus, one of the main challenges in airplanes context relies on ensuring coverage, requiring a thorough analysis of the communication channel.

For aircraft cabin context, first works have demonstrated diffuse optical transmission feasibility at speeds of up to 10 Mb/s [7], [9] considering a cellular communication scheme with several seat rows in each cell. In [11], an approach based on Monte-Carlo ray-tracing (MCRT) method has been used to investigate OWC performance including shadowing impact along predefined paths in aircraft cabin. In all these works, optical transceivers were fixed in the environment. In [12], we have studied for the first time in the literature, OWC channel for an aircraft cockpit with transceivers included in headset worn by the pilots. This environment not only presents a complex geometry, but also involves to take account for pilots' movements. The work in [12] was based on a modeling approach of optical waves propagation inside an Airbus A350 cockpit including pilot and co-pilot presence and head movements. We have studied connectivity between optical transceivers included on two pilot's headset and an access point (AP) located in the cockpit ceiling. The obtained results thanks to MCRT methodology and based on perfectly diffuse reflection models allowed determining the channel path losses considering head movements of the two pilots.

In this article, we first extend the study carried out in [12] by considering four pilots in the cockpit instead of two and by taking into account more complex movements involving the pilots' bodies. In addition, to be robust regarding head and body movements, we investigate spatial diversity contribution on the headset and assess the interest of this solution. For critical flight phases, such as take-off and landing, the brightness in the cockpit is reduced to accommodate pilots eyes in the dark, in the event of an electrical failure. To communicate in this context, the visible band is therefore not suitable, infrared (IR) is preferable, which differs from light fidelity systems (Li-Fi) exploiting both the lighting and communication functions [5]. Indeed, bidirectional Li-Fi transmissions consider the downlink in the visible range and the uplink conventionally in the IR, whereas we consider here the same IR wavelength for both links. In addition, Li-Fi technology generally involves high-speed applications, which is not the case for audio transmissions, conventionally requiring bitrates in the MHz range. For example, in the case of stereo audio signal sampled at 44.1 kHz over 16 bits, this corresponds to a required bitrate around 1.4 Mbps.

Based on the channel analysis, our objective is to study the performance of the bidirectional star network constituted of the four connected headsets and the AP located in the cockpit ceiling. Considering that pilots can use the headset in other environments than the cockpit, we are interested in the IEEE 802.11 channel access standard such as carrier-sense multiple access with collision avoidance (CSMA/CA). Indeed, there are currently standardization efforts on the commercial development of OWC technology, in particular Li-Fi [13], which aim at interoperability with Wi-Fi standards. One expectation is that the Li-Fi protocol can reuse the existing facilities within 802.11, such as distributed coordination function (DCF). In this work, we will consider the DCF algorithm with request to send/clear to send (RTS/CTS) method [14].

One main impact of channel access method is on delay between the acoustic signal and the audio management unit of the aircraft. Indeed, latency is a critical performance criterion for real-time audio quality in the cockpit and can have an impact on crew efficiency. Among the parameters contributing to audio latency, we focus here on the transmission time. For a given data packet size, the lower the rate, the higher the delay. To increase transmission rate, multi-carrier modulation schemes such as orthogonal frequency division multiplexing (OFDM) have been proposed for OWC systems, especially for Li-Fi technology due to their robustness face to inter-symbol interference (ISI) [5], [6]. But, it is at the cost of a high power consuming solution [15]. However, one main specification for audio headset is to guarantee sufficient autonomy to ensure long-haul flights. In order to respect this constraint, typical single carrier modulation schemes for OWC systems which are easy to implement and power efficient are considered [16], [17]. In addition, these modulation schemes are known to be suitable for low-medium data rate applications as the audio transmissions.

Consequently, another contribution of this paper is to highlight the trade-offs between minimal optical emitted power needed to attempt a given performance using typical OWC modulation schemes [16] and successful communication delay, considering a network based on IEEE 802.11 channel access mechanism with four optical wireless headsets and one AP inside the cockpit.

The remainder of the paper is organized as follows. Section II presents the description of cockpit environment including crew presence and the extended channel analysis. Section III then introduces the used modulation performance related to optical emitted power and the definition of communication delay regarding DCF with RTS/CTS method. Section IV shows the performance results and discussions before conclusion.

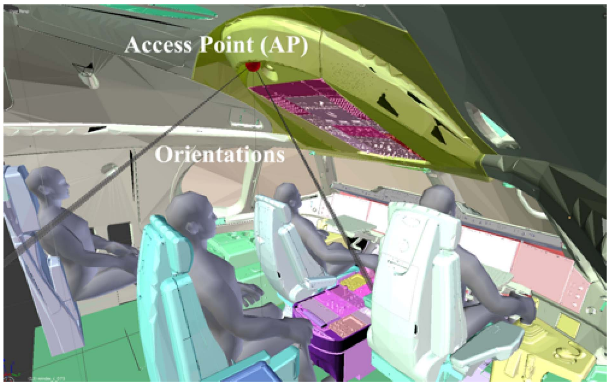

FIGURE 1. Location of the AP and occupant positions.

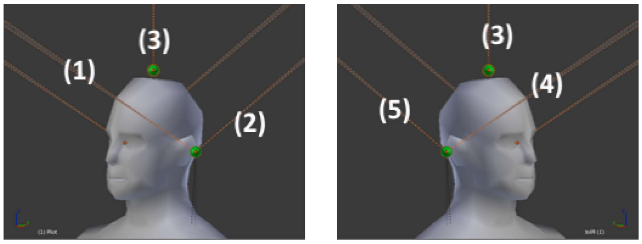

FIGURE 2. Orientations of Tx/Rx headset with spatial diversity.

II. COCKPIT ENVIRONMENT AND CHANNEL MODEL

A. ENVIRONMENT DESCRIPTION

The studied environment is the cockpit of an Airbus A350 aircraft. In this environment, we are focusing on a scenario using optical wireless links to ensure the connectivity of the headsets worn by the crew (pilot, co-pilot, third and fourth occupants). As said previously, we do not consider visible band because brightness in the cockpit is highly reduced during critical flight phases. Therefore, optical wavelength in the IR range at 940 nm is used.

We consider the IR bidirectional links between the transceivers (Tx/Rx) integrated on the headset and those located on the cockpit ceiling at the AP as illustrated in Fig. 1. Transmitter and receiver orientations at the AP (represented with grey lines in Fig. 1) are different according to the pilots. For the captain and first officer they are oriented between the two pilots, whereas for the third and fourth occupant at the cockpit rear the AP transceivers orientation is towards the cockpit door between the two pilots. In addition, as in [12], we have considered five possible locations and orientations of transceivers on the headset (see Fig. 2). This spatial diversity is investigated to increase robustness regarding head and body movements and have been chosen regarding integration feasibility over the headset. The Tx/Rx on the top of the head is named configuration 3. The two transceivers on the left ear are called configurations 1 and 2. The two symmetric ones located on the right ear are called configurations 4 and 5. Configurations 2 and 5 are oriented backward while configurations 1 and 4 are oriented towards the front. In the following, we will investigate performance according to transceiver configurations.

Moreover, note that the captain and first-officer seats have different settings linked to two extreme positions. The captain is furthest from the control panel (his/her face is at 60 cm) and his seat is as low as possible (the top of the head is 40 cm bellow the ceiling and 1.17 m above the floor). The first officer is on the contrary closest to the dashboard (his/her face is at 45 cm) and in a straight position so his head is at the greatest possible height (the top of his/her head is 15 cm below the ceiling, and 1.30 m above the floor). The head tops of the two first officers are located at about 1 m from the AP.

The third occupant (called the rear pilot) is located on the seat behind the captain and is the furthest from the AP (1.48 m), at 1.35 m above the floor and 55 cm below the ceiling. Finally, the fourth occupant (called the rear co-pilot) located behind the first officer is nearest from the AP (62 cm), at 1.3 m above the floor and 70 cm below the ceiling.

B. CHANNEL MODEL

Because of random movements of pilots, the line-of-sight (LOS) link condition cannot always be fulfilled. So, to determine the channel impulse response (CIR) for both uplink and downlink between the headsets and the AP, we have used the simulation software RaPSor (Ray Propagation Simulator) developed in our laboratory and already validated for optical waves propagation in indoor environments [18], [19]. It is based on a stochastic Monte-Carlo method, associated with the ray-tracing algorithm to numerically determine, from analytical models of reflection and propagation and for a defined link, the propagation delay and the received power for LOS and non-LOS (NLOS) paths, i.e., reflected paths over all the elements inside the cockpit. From this set of optical paths contributions, we then determine the CIR.

Thus, we have developed a detailed 3D geometric model of the cockpit (illustrated in Fig. 1) generated from a CAO file provided by AIRBUS, and then imported it into our software [12]. In addition, we have included the pilots bodies, fully articulated and animated using the Blender software [20]. The cockpit is a complex environment composed of surfaces and objects such as windscreen or crew bodies, having different optical reflection properties. Taking different behaviors for the cockpit surfaces requires modeling different bidirectional reflectance distribution functions (BRDF) which implies complex simulations. It was not the main objective of this study. Therefore, in our approach, for simplification reasons, all the cockpit and bodies surfaces are considered as perfectly diffuse and are consequently modeled using a Lambertian BRDF [19].

First, we consider that the reflectivity coefficients are set to 0.5, which is the mean value between absorbent and perfectly reflective material [12]. In Section IV-C, we will analyze the impact of reflectivity by considering additional extreme values equal to 0.1 and 0.9.

We have considered different scenarios for pilot movements, which cause random changes of headset

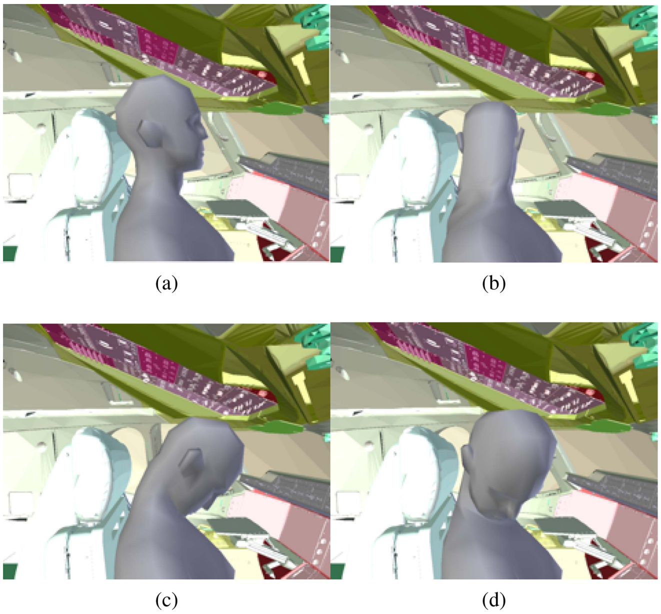

FIGURE 3. Illustration of head movement, frames (a) 1, (b) 4, (c) 7 and (d) 9.

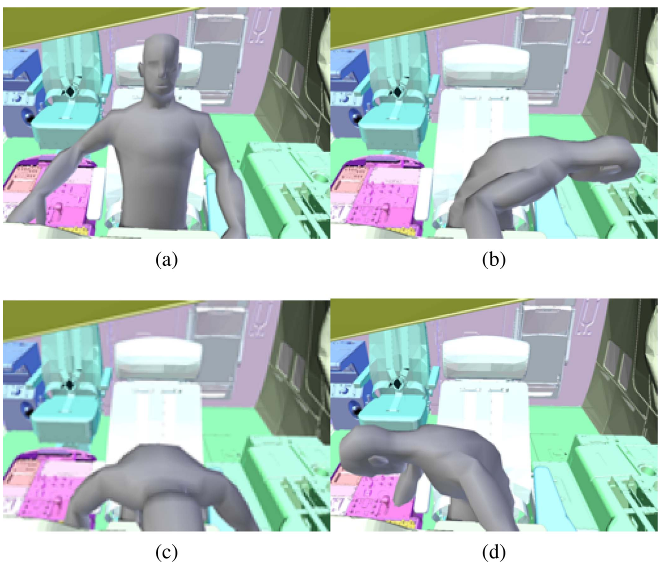

FIGURE 4. Illustration of body movement, frames (a) 1, (b) 4, (c) 7 and (d) 9.

transceivers orientation. The first one (head movement) supposes that a pilot looks ahead and then turns his/her head to the left, then tilts it forward, and then turns it to the right before returning it to its initial position. In the second scenario (body movement), a pilot leans to the ground to pick up a fallen object. Each movement (head and body) is discretized into 12 different frames. As an example, four of them (frames 1, 4, 7, and 9) are illustrated in Fig. 3 for head movement and Fig. 4 for body movement.

Each of these discretized movements induces different LOS and NLOS links according to the orientation changes of the headsets transceivers. This corresponds to a set of CIR $h(t)$.

TABLE 1. Maximum RMS delay spread τ_{RMS} (ns) among the four pilots. Transceivers on the top of the headset.

	Uplink	Downlink
Head movement	2.9	2.9
Body movement	3.1	3.2

To characterize the link, two parameters that are classically obtained from $h(t)$ are the DC gain H_0 and the root mean square (RMS) delay spread τ_{RMS} defined as [16]:

$$H(0) = \int_{-\infty}^{+\infty} h(t)dt = H_0 \tag{1}$$

$$\tau_{RMS} = \sqrt{\frac{\int_0^{+\infty} (t-\tau_0)^2 h^2(t)dt}{\int_0^{+\infty} h^2(t)dt}}, \tag{2}$$

with τ_0 the mean excess delay obtained from:

$$\tau_0 = \frac{\int_0^{+\infty} t h^2(t)dt}{\int_0^{+\infty} h^2(t)dt}. \tag{3}$$

The DC gain is one of the most important features representing the ratio between the received power P_r and the emitted one P_t. Moreover, to avoid inter-symbol interference (ISI), the delay spread should be significantly shorter than the symbol period T_s. We will consider that ISI can be neglected for symbol time T_s greater than 10 τ_{RMS}.

All the studied emitters are LEDs with optimal half-power semi-angles of 60° and 40° on headset and AP respectively, as established in [12]. Moreover, we use generic IR photodiodes with field of view of 60° (semi-angle at half power) and surface detection of 7 mm^2 for headset and AP receivers.

Considering the headset transceiver orientation, which randomly changes according to the head/body movements linked to the defined scenarios, we have first evaluated from simulation results the sets of corresponding H_0 and τ_{RMS} values. This has been done for both uplink and downlink for the 4 pilots and for the transceiver configuration 3 that is on the top of the headset (see Fig. 2).

Table 1 reports the maximum values of τ_{RMS} among all the obtained ones and for a reflectivity value equal to 0.5. In downlink, the maximum values of τ_{RMS} reported are obtained for the captain head movement and the rear co-pilot body movement respectively.

To illustrate the impact of the movements on the CIR, Fig. 5 shows the example of the downlink between the AP and the headset worn by the captain. Fig. 5 (a) corresponds to the case where the captain is in a straight position in his seat and Fig. 5 (b) to the case with a head movement (frame 4, see Fig. 3) which corresponds to the maximum τ_{RMS} value of Table 1. In addition to the CIR drawn in solid line, the different optical contributions are given as a function of the reflection depth. It can be seen in Fig. 5 (a) when the captain's head is straight, that the LOS contribution dominates widely and leads to a very low τ_{RMS} value equal to 37 ps. A zoomed view of the black circled zone proposed in Fig. 5 (a) allows noting that the contributions once reflected

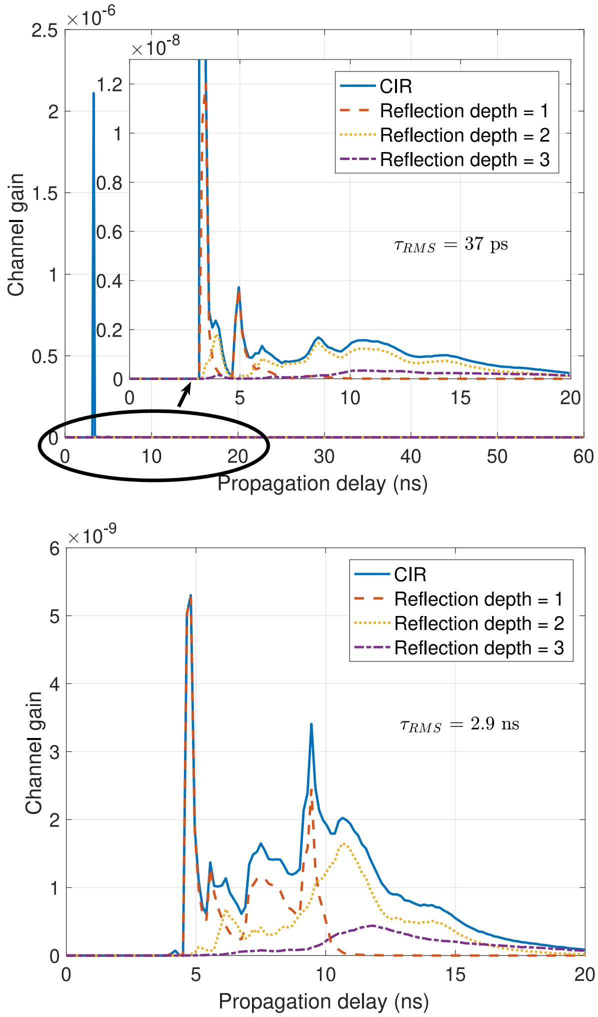

(a)

(b)

FIGURE 5. CIR for downlink and captain (a) in straight position and (b) with head position corresponding to the maximum τ_{RMS} in Table 1.

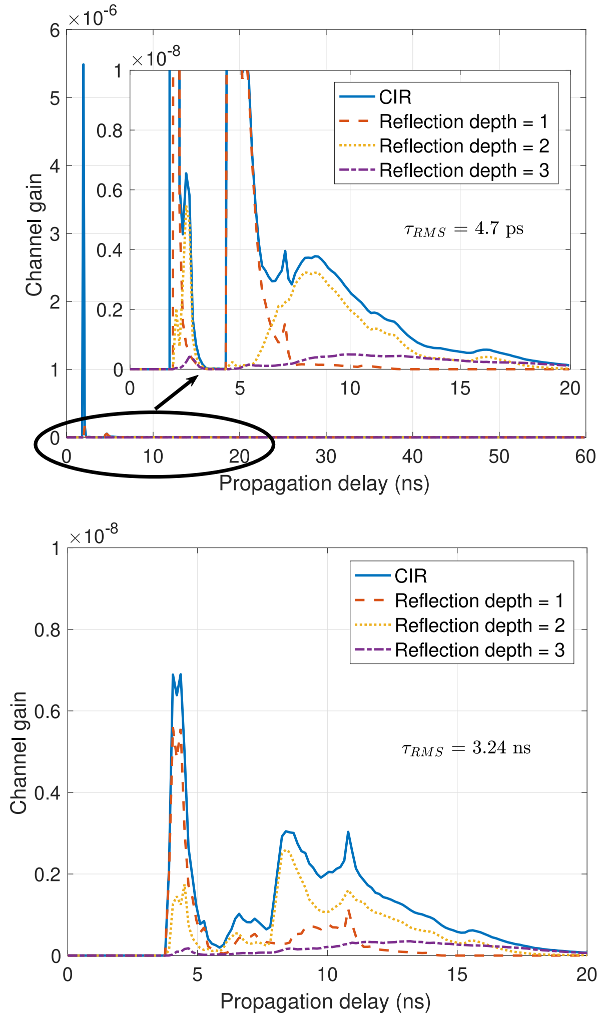

(a)

(b)

FIGURE 6. CIR for downlink and rear co-pilot (a) in straight position and (b) with body position corresponding to the maximum τ_{RMS} in Table 1.

are first dominant between 3 and 6 ns, then are dominated by those twice reflected, the third low reflected contribution being mainly present between 7.5 ns and 20 ns. In Fig. 5 (b) the CIR for the captain head movement corresponds to the maximum τ_{RMS} value. Indeed, we can note that in this case, the LOS link is blocked, leading to an increased τ_{RMS} of 2.9 ns as seen in Table 1. Exactly same behavior is observed for the rear co-pilot body movement in downlink. In Fig. 6 (a) corresponding to the case where the rear co-pilot is in a straight position, LOS path dominates. On the contrary, the blockage of the LOS link due to body movement leads to an increase of the τ_{RMS} value from 4.7 ps to 3.2 ns as illustrated in Fig. 6 (b).

From the overall results of Table 1, we can see that the time dispersion induced by the reflected paths is very low. This allows neglecting ISI for symbol time greater than 32 ns that corresponds to symbol rate around 30 Mbps for single carrier modulations.

In addition, to investigate the performance of the network constituted of the four headsets and the AP, we consider that the system should be able to work for the lowest gain values among all the possible values linked to the pilot's movements, so that the network is reliable in the worst case. The lowest gain values H_0 in dB among the head/body movements, for each pilot and considering transceiver configuration 3, are reported in Table 2 for a reflectivity value of 0.5.

We first observe that the head movements are the most penalizing for the headsets worn by the captain and the first officer while for the rear occupants it is the body movements.

In addition, for captain and first officer headsets the lowest DC gains are obtained in uplink whereas this is in downlink for rear pilot and rear co-pilot. Finally, considering all the cases, the worst corresponds to the bidirectional link of the rear co-pilot headset with body movements (in bold in Table 2).

As mentioned in Section II-A, different transceivers positions and orientations on the headset can be investigated in addition to that on the top of the head, i.e., configurations 1 to 5 (see Fig. 2). The idea is to take advantage of spatial

TABLE 2. Lowest DC gain (dB) among the four pilots. Transceivers on the top of the headset.

	Uplink head mvt.[1]	Uplink body mvt.	Downlink head mvt.	Downlink body mvt.
Captain	-70.3	-69.4	-69.7	-69.2
First officer	-72.1	-71.9	-71.2	-70.1
Rear pilot	-66.3	-67.9	-68.4	-68
Rear co-pilot	-61.1	**-72.2**	-52.7	**-74**

[1] mvt. is for movement.

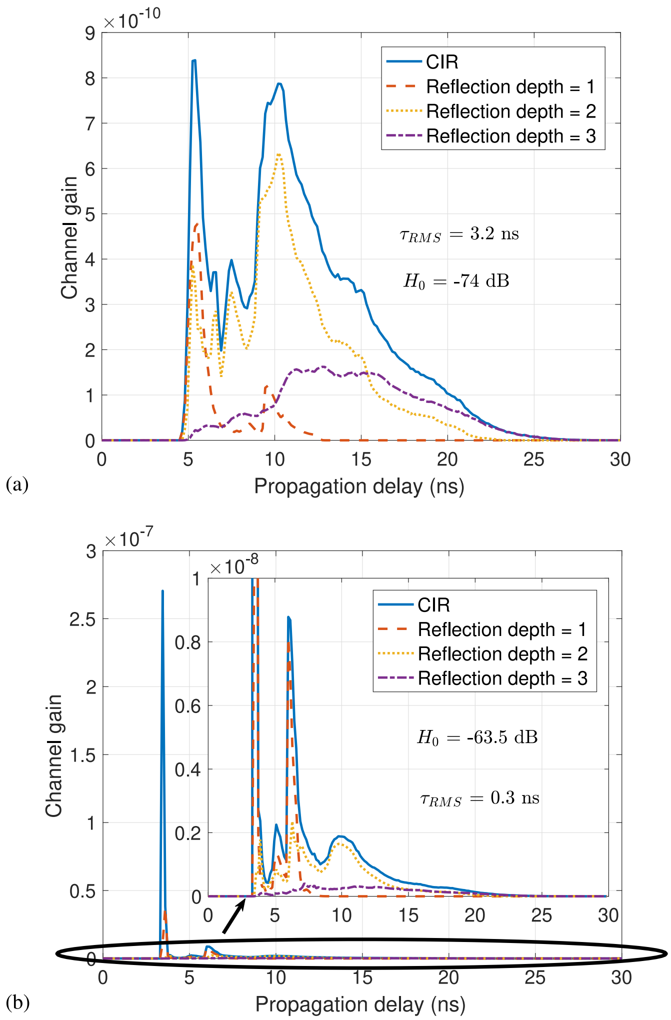

FIGURE 7. CIR corresponding to the frame 9 of the body movement for rear co-pilot downlink and transceivers (a) configuration 3, (b) configuration 5.

diversity to improve link robustness regarding LOS blockage due to head and body movements. This is illustrated in Fig. 7 (a) and (b) which present the downlink CIRs of the rear co-pilot corresponding to the frame 9 of the body movement (see Fig. 4), obtained for the headset's transceivers

TABLE 3. Lowest DC gain (dB) among the transceivers configurations for the rear co-pilot.

	Uplink	Downlink
Configuration 1, left ear	-72.9	-75.3
Configuration 2, left ear	-63.9	-65.5
Configuration 3, head top	-72.2	-74
Configuration 4, right ear	-71.1	-73.1
Configuration 5, right ear	**-63.3**	**-63.5**

TABLE 4. Lowest DC gain (dB) used for network performance.

	Uplink	Downlink
1 Tx/Rx, 2 pilots	-72.1	-71.2
3 Tx/Rx, 2 pilots	-68.2	-67
1 Tx/Rx, 4 pilots	-72.2	-74
3 Tx/Rx, 4 pilots	-68.2	-67

configurations 3 and 5 respectively. We can see that configuration 5 (Fig. 7 (b)) leads to a high increase of received optical power (10.5 dB) compared to the configuration 3 (Fig. 7 (a)). This is due to the LOS contribution, which is not blocked with configuration 5 unlike configuration 3, but also to the reflected paths which are approximately 10 times greater. In addition, we can remark that configuration 5 also leads to a decrease of the τ_{RMS} value.

Hence, we have made the same analysis regarding head and body movements as the one presented in Table 2, but considering the other transceiver configurations as defined in Fig. 2. As an example, Table 3 reports for the rear co-pilot the lowest DC gain values according to the transceiver configurations. As expected, we can see that the gain values can be enhanced thanks to spatial diversity. For the example reported in Fig. 7, the gain value is of -63.5 dB with a receiver on the right ear (configuration 5) instead of -74 dB with the receiver on the top of the headset (configuration 3). This means that for rear co-pilot, the best downlink performance can be established using the receiver in configuration 5. We have performed the same analysis for the other pilots. The obtained results are reported in the Appendix.

We can note that depending on the pilot location and on uplink or downlink transmission, an optimal transceiver configuration is either 2, 3 or 5. Configurations 1 and 4 do not bring any improvement. Therefore, we can conclude that, among the tested transceiver configurations, the optimal headset should include 3 Tx/Rx placed according to these 3 configurations. After reception of the signals from the 3 configurations, combining techniques can be implemented in order to efficiently recover the emitted information. In this work, results are presented considering the signal having the maximal strength (maximal gain value) among theses 3 configurations. This corresponds to selection combining (SC) method [21]. This is not the optimal combining technique but one of the simplest to implement. In order to evaluate the performance in the worst configuration, we have extracted from tables in the Appendix the lowest gain values for both uplink and downlink considering 1 Tx/Rx (on the top of the headset, i.e., configuration 3) and 3 Tx/Rx (configurations 2, 3 and 5) with SC method. These worst gain values are summarized in Table 4 and are used in the following of this article to evaluate link performance. Note that with diversity, the gain improvement is at least of 4 dB for both links.

With 1 Tx/Rx as seen previously in Table 2, the limiting gain is due to first officer headset when considering 2 pilots and to rear co-pilot one with 4 pilots in the cockpit. Furthermore, the lowest gain values for 2 pilots wearing headsets with 3 Tx/Rx are −68.2 dB and −67 dB for uplink and downlink respectively. These two values correspond to transceivers located on the left ear of the first officer and oriented backward (configuration 2). The lowest gains are identical for 4 pilots, always corresponding to a transceiver on the left ear of the first officer (configuration 2). The overall limiting gain in this case is therefore due to the first officer.

III. EMITTED POWER AND COMMUNICATION DELAY

In this section, we first consider the emitted power required to attempt a given *BER* for classical optical modulation schemes. Then, to determine the delay, we describe the multi-user medium access control mechanism that is DCF algorithm with RTS/CTS method. As the delay diminishes with the data rate, while the required power increases, our objective is to analyze the trade-offs for OWC-based audio transmission inside aircraft cockpit.

A. EMITTED POWER

The channel analysis has been performed in previous section in term of optical DC gain. For a fixed emitted power P_t, the signal to noise ratio (*SNR*) is expressed as [16]:

$$SNR = \frac{H_0^2 P_t^2 R^2}{\sigma^2}, \tag{4}$$

where R is the photodiode responsivity and σ^2 is the total noise variance. R is set in the following to 1 A/W to normalize the *SNR* values in order to obtain a generic approach, independently of the considered photodiode. Thus, evaluating the *SNR* according to a specific photodiode will just consist in multiplying the DC gain by the considered R value. Concerning the noise, it is traditionally assumed that the dominant noise sources in an indoor OWC system are the background light-induced shot noise and the receiver thermal noise [22]. Shot noise is generally recognized as the most limiting factor [16], considered as an additive white gaussian noise (AWGN), with σ^2 approximated by:

$$\sigma^2 = 2qI_bB, \tag{5}$$

where q is the electron quantum charge and B the bandwidth of the modulated signal equal to the symbol rate. For ambient photocurrent I_b, we consider the measured value provided by Moreira *et al.* in [23] according to IR domain, which is 200 μA.

Moreover, *BER* performance of typical modulation schemes depends on *SNR*. On-off keying (OOK) and pulse position modulation (PPM) are single-carrier formats classically used for IR communication systems [22].

TABLE 5. DCF specifications.

Attributes	Values
RTS (s)	288 (bits)/R_b
CTS (s)	240 (bits)/R_b
ACK (s)	240 (bits)/R_b
Data (s)	(MDPU+128)(bits)/R_b
Media access control protocol data unit MDPU (bytes)	[0, 2500]
DIFS (μs)	26
SIFS (μs)	10
Time slot duration N_s (μs)	8
$CW_{\min}$ (integer)	63
$CW_{\max}$ (integer)	1023

For OOK modulation, the *BER* is expressed as follows:

$$BER_{OOK} = \frac{1}{2} erfc\left(\sqrt{\frac{SNR}{2}}\right). \tag{6}$$

L-level PPM is a power-efficient modulation scheme, which is of main interest regarding the use-case of audio headset needing supply autonomy for long-flight. L-PPM maps M bits into a single pulse placed at one of the $L = 2^M$ possible locations or slots. It has been shown [6], [22] that its *BER* is obtained from:

$$\begin{aligned} BER_{L-PPM} &= \frac{\frac{L}{2}}{L-1} P_{sye-PPM} \\ P_{sye-PPM} &= 1 - (1 - P_{sle-PPM})^L \\ P_{sle-PPM} &= \frac{1}{2} erfc\left(\frac{\sqrt{L.SNR.M}}{2}\right), \end{aligned} \tag{7}$$

where $P_{sye-PPM}$ is the symbol error rate and $P_{sle-PPM}$, the slot error probability.

By exploiting the expressions (6) and (7) for OOK and L-PPM, we can determine the targeted values of *SNR* for a given *BER* performance level. Then, by using the DC gain values of Table 4, it is possible to obtain the requested P_t value for the studied system according to the data rate R_b.

B. COMMUNICATION DELAY

To ensure multi-user communication, we propose an approach based on 802.11 medium access control mechanism. We are interested in the DCF basic method, used for 802.11 devices [14] and investigated for Li-Fi [24]. The DCF method is known as carrier sense multiple access with CSMA/CA mechanism.

With the basic DCF access method, if the channel is free for the transmitters, each one randomly chooses a waiting slot called backoff contention windows (*CW*) which is in the interval [$CW_{\min}$, $CW_{\max}$]. The waiting time is thus obtained by *CW* multiplied by the time slot duration N_s defined by the standard (see Table 5).

TABLE 6. Network parameters.

Attributes	Values
n	3 and 5
m	1
p	0% and 5%

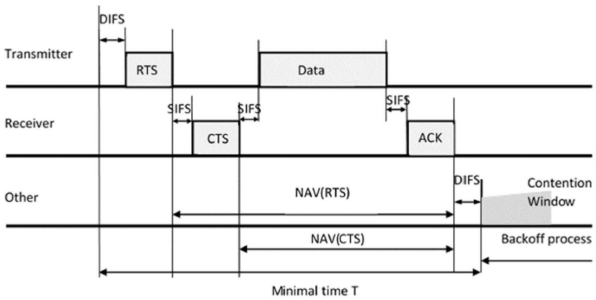

FIGURE 8. Principle of DCF mechanism with RTS/CTS.

As long as the channel is detected idle for a time slot, the backoff is decreased by one. The communication begins when the backoff value is null and if the channel is free. When the channel is busy, the time counter is blocked and resumed when the channel is inactive again for at least one time slot.

One strong limitation of DCF arises from the obligation to send a request to the physical layer to know if the channel is free. Indeed, the node has to be able to listen to the channel. This is the well-known issue of hidden nodes, which can be relaxed by the use of RTS/CTS mechanism, which is optional in WLANs but mandatory in optical wireless networks [24]. The trade-off is additional RTS/CTS frames exchange introducing transmission overhead.

The scenario of the RTS/CTS process is illustrated in Fig. 8. The sending node uses an RTS frame for the receiver node after a distributed inter-frame space (DIFS) waiting time. The other nodes present in its coverage area receive this frame and initialize their network allocation vector (NAV) counter. During NAV time, they know that they cannot transmit frames at the risk of causing collisions. The receiving node responds after a short inter-frame space (SIFS) with a CTS frame. Other nodes present in its CTS coverage area initialize their NAV. If the listening of the channel goes well, the sending node waits for the SIFS duration and sends a data frame. An acknowledgment ACK is received after a short SIFS period if the transmission is correct.

Table 5 contains the specifications for the DCF method with RTS/CTS that we consider where R_b is the PHY data rate. The values of RTS, CTS, ACK and Data take into account the PHY overhead.

The metrics usually used to analyse the network performance are throughput and delay. We consider an analytical approach to evaluate these criteria, based on the Bianchi [25] model and its extension proposed in [26]. In these models, the time slot duration N_s indicates the time during which a node needs to detect the transmission of other nodes [26].

It is assumed that a node transmits in a time slot randomly chosen with a probability τ. The packet being transmitted experiences a collision with a probability p.

These two parameters are the main features of binary exponential-backoff (BEB) algorithm in DCF [25]. Considering a given number of attempts m, the probabilities τ and p are given by [26]:

$$\tau = \frac{2}{1 + CW + pCW \sum_{i=0}^{m-1} (2p)^i}$$
$$p = 1 - (1-\tau)^{n-1}, \tag{8}$$

where n is the number of nodes. This assumes that at least one of the $(n-1)$ remaining nodes transmits in a given time slot.

The probability P_{tr} that there is at least one transmission in the considered time slot is expressed as [25], [26]:

$$P_{tr} = 1 - (1-\tau)^n. \tag{9}$$

In [25], [26], the probability P_s that a transmission occurring on the channel is successful is given by:

$$P_s = \frac{n\tau(1-\tau)^{n-1}}{P_{tr}}. \tag{10}$$

During the mean time T_{succ}, expressed in (11), the channel is detected as busy due to a successful transmission. In addition, during the average time T_{col}, the channel is detected as busy because a collision occurred during the transmission attempt [25]:

$$T_{succ} = RTS + CTS + Data + ACK + 3SIFS + DIFS$$
$$T_{col} = RTS + DIFS + SIFS + CTS. \tag{11}$$

The delay of a successfully transmitted packet D_{succ} can be obtained from [26]:

$$D_{succ} = L_{slot} N_{slot}, \tag{12}$$

where L_{slot} is the average length of a time slot and N_{slot}, the average number of time slots for a successful packet transmission. L_{slot} is expressed as follows [26]:

$$L_{slot} = P_{idle} N_s + P_{succ} T_{succ} + P_{col} T_{col}. \tag{13}$$

In [25], [26], the probabilities P_{succ} and P_{col} are respectively expressed as:

$$P_{succ} = P_{tr} P_s$$
$$P_{col} = P_{tr} - P_s. \tag{14}$$

The probability P_{idle} of having a randomly chosen idle slot is obtained from [25], [26]:

$$P_{idle} = 1 - P_{tr}. \tag{15}$$

N_{slot} is expressed as follows [26]:

$$N_{slot} = \frac{(1+CW)(1-2p) + CWp(1-(2p)^m)}{2(1-2p)(1-p)}. \tag{16}$$

In the following, we determine the successful delay D_{succ} defined in (12), using the DCF parameters of Table 5.

IV. PERFORMANCE ANALYSIS

In order to evaluate performance taking into account both PHY and MAC layer metrics, considering classical binary symmetric channel, we consider the packet error rate (*PER*), where packets are formed with N transmitted symbols. Without any coding on this packet, *PER* at a given instantaneous *SNR* is given by [27]:

$$PER = 1 - (1 - BER)^N. \tag{17}$$

The *BER* is a PHY layer metric, linked to the optical emitted power. The number of bits N is the packet size. This is a MAC layer parameter.

In the aeronautical context, a strong requirement for the end user is the robustness of the wireless transmission in terms of *PER* which must be guaranteed during the pilot's movements, as there is no possibility to resend lost packets. Thus, *PER* metric can be considered as a cross-layer PHY/MAC metric from which we will be able to discuss on the trade-offs between emitted power and delay of successful transmission.

A. EMITTED POWER P_T FOR A TARGETED QUALITY OF SERVICE

From (6)-(7), we can compute the *BER* as a function of the *SNR* for OOK and *L*-PPM modulations. Then, using (4)-(5) we determine the required P_t value to reach a given *SNR* so *BER*, according to data rate R_b.

In this section, we consider the worst DC gain values reported in Table 4 for uplink and downlink with 1 and 3 Tx/Rx with SC method, and for 2 and 4 pilots respectively.

Considering the maximal media access control protocol data unit (MPDU) size from specifications reported in Table 5 (2500 bytes, so N = 2500*8 bits) and a targeted *PER* of 10^{-3}, this corresponds to a *BER* of around 5.10^{-8}. For this *BER* value, the minimal emitted power P_t is determined as a function of the data rate and reported in Fig. 9 (a) and (b), for 2 and 4 pilots respectively. The results have been obtained for OOK and 4-PPM with 1 and 3 Tx/Rx.

As expected, for a given performance and in all cases, increasing the data rate R_b requires increasing the emitted power.

If we focus on the case with 2 pilots in Fig. 9 (a), we can note that uplink always requires more power than downlink in order to reach a given data rate. For example, from Fig. 9 (a) considering OOK we can see that for R_b equal to 2 Mbps, a power of nearly 1 and 0.8 W is required for uplink and downlink respectively. On the contrary, with 4 pilots and 1 Tx/Rx in Fig. 9 (b), we notice that the downlink is more power consuming, but that required power for uplink is quite the same as for 2 pilots. Finally, for the case with 4 pilots and 3 Tx/Rx in Fig. 9 (b), the curves are identical to those of Fig. 9 (a). This is consistent with the DC gain values in Table 4.

In addition, we can note that the required power with OOK modulation is higher than with a 4-PPM for both uplink and downlink configurations, regardless the number of pilots.

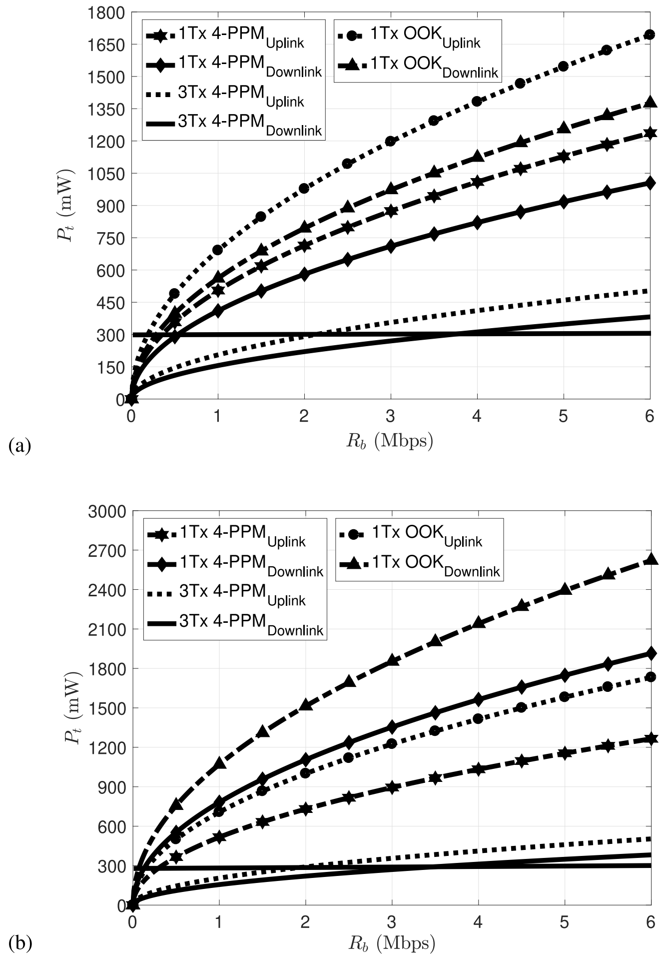

FIGURE 9. Emitted power P_t according to data rate R_b. *PER* equal to 10^{-3}, for (a) 2 and (b) 4 pilots.

This confirms the power efficiency of 4-PPM modulation over OOK. For example, in Fig. 9 (b), for R_b equal to 1 Mbps, the required power is 517 mW with 4-PPM and 710 mW with OOK for the uplink with 1 Tx/Rx.

Thus, in the following, we only focus on 4-PPM modulation. By comparing the curves with and without diversity, we can observe as expected, that the use of diversity improves performance. Indeed, for a given data rate, the required powers are lower when we consider 3 Tx/Rx instead of 1 Tx/Rx. This remark is truer for the downlink than for the uplink. Furthermore, it can be noted that the curves for the two links are quasi-identical in the case with diversity. This is an interesting result, which can facilitate the development of the system.

Finally, we must take into account the fact that the IR emitted power is limited by the eye safety criterion defined in the available standards. For laser equipment, the basic standard is the IEC 60825-1 [28]. For lamps and LEDs, which are incoherent broadband optical sources, it is the IEC 62471 [29]. Having a wide opening, LEDs considered in the study must respect the second standard where limitation is less restrictive than IEC 60825-1. In particular,

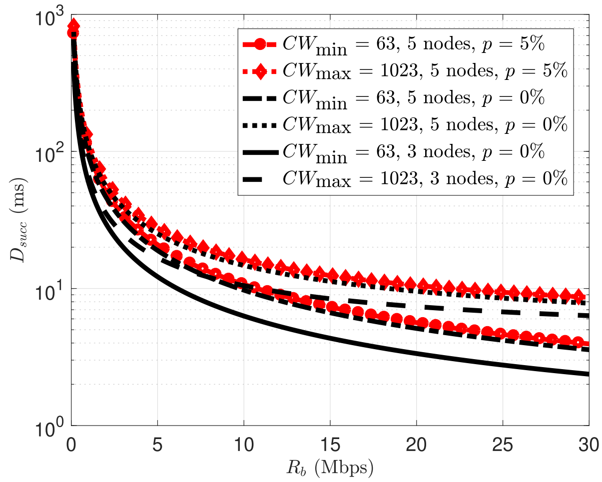

FIGURE 10. Successful delay D_{succ} according to data rate R_b, MPDU = 2500 bytes, CW_{min} = 63, CW_{max} = 1023, 3 and 5 nodes.

for the 940 nm wavelength, [29] imposes an irradiance of 100 W.m^{-2} at a distance of 20 cm, leading to a limit value of optical emitted power of about 12.5 W and 7 W for uplink and downlink respectively.

In our analysis, for supply autonomy reason, we consider, in a first analysis, a more restrictive IR limitation of 300 mW. Using this limit value, we can extract from Fig. 9 (a) and (b) the maximal data rates in the case of 3 Tx/Rx, for 2 and 4 pilots respectively. For 2 pilots, it corresponds to 3.69 and 2.12 Mbps for downlink and uplink respectively, whereas it is 3.69 and 2.12 Mbps for 4 pilots. Another important performance indicator depending on the data rate is the transmission delay, as presented in the next section.

B. SUCCESSFUL TRANSMISSION DELAY FOR A TARGETED QUALITY OF SERVICE

The network is constituted of 3 or 5 nodes, corresponding to the AP plus 2 or 4 pilots respectively. From expressions established in Section III, the evolution of the delay is reported in Fig. 10 as a function of the data rate R_b for network parameter values summarized in Table 6 and for the two-extreme contention window values *CW* equal to 63 and 1023. Moreover, we have considered weak values of collision probability p (0% and 5%), since we are studying a network with a very low number of nodes [26].

As expected, we observe in Fig. 10 that the delay D_{succ} decreases as R_b increases regardless the number of nodes. For a data rate of 2 Mbps and 5 nodes, it reaches values around 45 ms and 55 ms, for CW_{min} and CW_{max} respectively. In this case, the contention window variation has an impact of about 18% on the delay. Concerning the collision probability p, we observe that the delay D_{succ} slightly increases with p. For example, if we consider 2 Mbps, CW_{max} and 5 nodes, the delay is equal to 57 ms when considering p equal to 0% whereas it is of 62 ms when considering p equal to 5%. This represents an increase of about 8%. It is a low impact so we have supposed in the following that there is no collision. With this simplification, we consider a successful transmission from the first attempt ($m = 1$).

TABLE 7. Delay D_{succ}, for 4-PPM modulation, P_t equal to 300 mW and 5 nodes.

	Maximal data rate R_b	CW_{min} = 63	CW_{max} = 1023
MPDU 2500 bytes	3.69 Mbps, 3 Tx/Rx for downlink	26 ms	33 ms
	2.12 Mbps, 3 Tx/Rx for uplink	44 ms	54 ms
	140 kbps, 1 Tx/Rx for downlink	660 ms	745 ms
	330 kbps, 1 Tx/Rx for uplink	280 ms	219 ms

TABLE 8. Delay D_{succ}, for 4-PPM modulation, P_t equal to 300 mW and 3 nodes.

	Maximal data rate R_b	CW_{min} = 63	CW_{max} = 1023
MPDU 2500 bytes	3.69 Mbps, 3 Tx/Rx for downlink	17 ms	22 ms
	2.12 Mbps, 3 Tx/Rx for uplink	28 ms	34 ms

For data rates lower than 2 Mbps, the delay increases, but the relative variation is lower. For example, for R_b equal to 0.6 Mbps and 5 nodes, the delay varies from 155 ms to 178 ms according to *CW*. This corresponds to 13% of increase between the minimal *CW* value and the maximal one.

Concerning the number of nodes, we observe that the delay D_{succ} increases when it goes from 3 to 5. For example, if we consider 1 Mbps and CW_{max}, we can see from the results in Fig. 10 that the delay is 67 ms when considering 3 nodes whereas it is 108 ms when considering 5 nodes. This represents an increase of about 38%, which is a more significant impact compared to *CW* or collision probability ones.

To reduce the delay regardless the number of nodes, the data rate can be increased, but we can see in Fig. 10 that the curves converge. Note that due to the value of CW_{max} equal to 1023, the minimal achievable delay value is of 4.38 ms. In addition, the increase in data rate is limited by the power value as indicated in previous Section IV-A.

C. TRADE-OFFS DISCUSSION

To illustrate the trade-offs between emitted power and successful transmission delay, we first consider in this analysis 4-PPM modulation with an emitted power of 300 mW for the case with 4 pilots.

From the maximal achievable data rates in Fig. 9 (b) corresponding to a targeted PER of 10^{-3} according to 1 Tx/Rx and 3 Tx/Rx respectively, we have reported in Table 7, the delay obtained for $n = 5$ from Fig. 10. The MPDU size is of 2500 bytes and we have considered the two extreme values of *CW*.

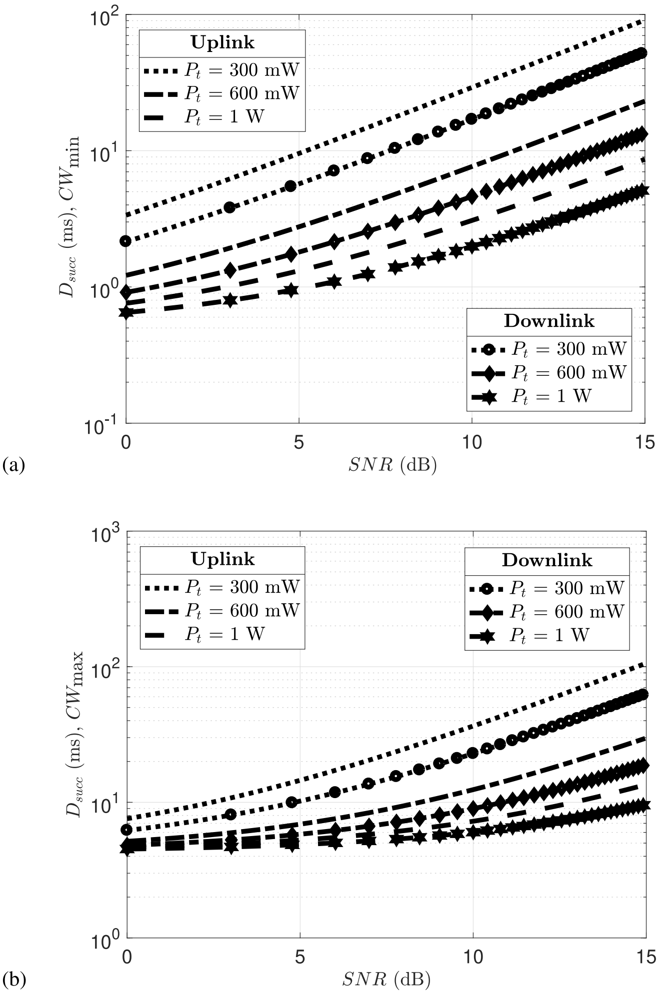

FIGURE 11. Successful delay D_{succ} according to SNR, for MPDU = 2500 bytes, 5 nodes and (a) $CW_{\min}$ = 63 and (b) $CW_{\max}$ = 1023.

First, we can notice that the maximal data rate and so the corresponding delay for the case without diversity are much lower than with diversity. Indeed, considering the 3 Tx/Rx on the headset, a maximal delay of 54 ms can be guaranteed for successful transmission instead of 745 ms with 1 Tx/Rx. This value corresponds to the uplink with the lowest gain as seen in Table 4.

Note that if the packet size is reduced, this value can be obviously lowered. For example, if the packet size is divided by 100 (25 bytes), the obtained value is diminished by 88% so around 6 ms.

To illustrate the impact of the number of pilots, we have reported in Table 8 the delay in the case 3 Tx/Rx for 2 pilots. As expected, we verify that the maximal delay is lowered. The uplink imposes the guaranteed value of 34 ms instead of 54 ms for 4 pilots.

To present the results more generally with 3 Tx/Rx and 5 nodes, we have plotted in Fig. 11 the evolution of the delay, as a function of the SNR defined by equations (4) and (5) where the bandwidth B is equal to R_b. This has been done for different emitted power values and considering a MPDU size of 2500 bytes. Fig. 11 (a) and (b) correspond to $CW_{\min}$ and $CW_{\max}$ respectively.

TABLE 9. Required P_t for 4-PPM modulation, 3 Tx/ Rx, MPDU = 2500 bytes and 4 pilots.

		$CW_{\min}$ = 63, B = 19.4 MHz	$CW_{\max}$ = 1023, B = 36.7 MHz
D_{succ} = 10 ms	Downlink	486 mW	668 mW
	Uplink	641 mW	944 mW

TABLE 10. Delay D_{succ}, according to different targeted PER, P_t = 300 mW, MPDU = 2500 bytes and 4 pilots.

	R_b	$CW_{\min}$ = 63	$CW_{\max}$ = 1023
4-PPM	B = 6.44 MHz, 3 Tx/Rx for downlink, $PER = 10^{-4}$	30 ms	37 ms
	B = 7.38 MHz, 3 Tx/Rx for downlink, $PER = 10^{-3}$	26 ms	33 ms
	B = 8.68 MHz, 3 Tx/Rx for downlink, $PER = 10^{-2}$	22 ms	29 ms
	B = 19.52 MHz, 3 Tx/Rx for downlink, $PER = 10^{-1}$	18 ms	24 ms

TABLE 11. Delay D_{succ}, according to reflectivity value ρ, $PER = 10^{-3}$, MPDU = 2500 bytes, 3 Tx/ Rx, $CW_{\max}$ = 1023, P_t = 300 mW and 4 pilots.

	ρ	Downlink
4-PPM	0.1	6483 ms
	0.5	33 ms
	0.9	11 ms

Considering a targeted PER, i.e., a targeted BER for 2500 bytes, one can determine from the SNR the corresponding successful delay according to the emitted power. As an example, for a PER of 10^{-3} therefore a BER of 5.10^{-8}, the corresponding SNR for 4-PPM is 8.79 dB using equation (7). As the required bandwidth of 4-PPM is $B = 2\ R_b$, we have considered a SNR of 11.79 dB in Fig. 11 (b), which corresponds to a delay of 54 ms for the uplink with a power of 300 mW. This is consistent with the result shown in Table 7. Thus we can use Fig. 11 to discuss the trade-offs for different modulation orders, targeted PER, maximal admissible delay or emitted power.

First, considering the requirements specified in the DO-214 standard [30] for the aircraft audio systems, a delay of 10 ms appears as an upper bound value. For a PER of 10^{-3} with 4-PPM that is a SNR of 11.8 dB, one can extract from Fig. 11 (a) and (b) the emitted power for this delay. Values are reported in Table 9 for both uplink and downlink. We have also reported the corresponding values of bandwidth. We can see that power values are much higher than the considered 300 mW, but respect the safety limitations imposed by [29]. This allows considering system implementation in a cockpit but requiring feasibility study in terms of consumption for a long flight use. However, the bandwidth for $CW_{\max}$ shows that we tend towards the limit for which we can no longer neglect the ISI.

Then, we analyse in the following the impact of targeted *PER* and higher order PPM modulation on the emitted power, thus on the delay. In addition, we will also illustrate how performance is affected for different reflectivity values.

For different targeted *PER* with 4-PPM modulation, we have determined the associated *SNR* and extracted from Fig. 11 the corresponding delay for an emitted power of 300 mW for the downlink as an example. The results are reported in Table 10.

We can observe from values in Table 10 that reducing the constraint on targeted *PER* by one decade (*PER* equal to 10^{-2}) allows to lower the delay by approximately 15%. On the other hand, the delay is increased by about 11% when the *PER* is 10^{-4}. These variations are relatively small and we can therefore conclude that the value of *PER* does not have a preponderant impact on the delay.

For 16-PPM and the targeted *PER* of 10^{-3}, knowing that the required bandwidth is $B = 4R_b$, we consider a SNR of 6.07 dB. Thus for a given emitted power, the corresponding delay will be lowered compared to 4-PPM. Moreover, from Fig. 11 (b) and for a delay of 10 ms, this *SNR* leads to an emitted power around 456 mW instead of 944 mW with 4-PPM as shown previously in Table 9. Indeed, using 16-PPM allows highly reducing the power or the delay but at a cost of a high bandwidth, so potential ISI. In addition, a higher order of PPM modulation implies an increase of the implementation complexity and therefore greater consumption, which is not desirable.

All the results were obtained considering an average value of 0.5 for environment's and bodies' reflectivity. To complete the analysis, we have reported in Table 11 the delays obtained for extreme reflectivity values of 0.1, corresponding to absorbent surfaces, and 0.9 corresponding to quasi perfectly reflective ones. The results show that the impact of the reflectivity is rather exponential. However, it is not realistic to consider that all surfaces and objects in the cockpit are either fully blocking or reflecting. One perspective would be to take into account the nature of the different surfaces and objects, which requires modeling different BRDFs, and therefore a complex simulation as in [31].

V. CONCLUSION

In this article, we have studied a network composed of four audio headsets connected in optical wireless and an AP located at the cockpit ceiling of an Airbus A350. The main objective was to study the trade-offs as a function of the data rate linked to the physical channel parameters, in particular the transmission power, and to those resulting from the channel access method based on DCF with RTS/CTS.

We first studied the modelling of the channels for uplink and downlink between the headsets and the AP. This contribution was based on the advanced cockpit simulation from a 3D geometric model of the cockpit. In addition, the presence of the pilots and their movements were taken into account. Simulation of the channel by ray tracing associated with a Monte-Carlo method allowed determining the gain values of the channel in the worst case to consider full reliability in both uplink and downlink. For the transceivers on the top of the headset, the results show that the worst case corresponds to the position of the rear co-pilot. We have also pointed out that by using spatial diversity including three transceivers respectively on the head top, right and left ears and the SC method, it is possible to enhance the gain performance. A perspective to improve the performance linked to diversity could be to use more sophisticated combining techniques, by studying the trade-offs with the complexity increase.

Based on channel analysis, we then performed a combined study of the transmitted power and the delay for successful communication. The minimum optical power necessary for a given performance has been evaluated for conventional OWC modulation schemes (OOK and PPM) as a function of the data rate. Likewise, we have studied the delay values for successful communication in the network for the studied protocol and for a given emitted power regarding eye safety regulations and headset autonomy constraints. We have shown that using headsets with transceiver diversity allows reaching a delay much lower than without diversity.

Furthermore, very low delays can be guaranteed according to the packet size or the power. Thus, the approach has highlighted the trade-offs between power and delay linked to achievable data rate for a given performance. Finally, we have shown that increasing the order of the modulation is the most effective way to reduce the delay or the power but at the cost of an implementation complexity increase and potential ISI.

APPENDIX
MINIMAL DC GAIN FOR THE OTHER CREW MEMBERS

In the case of the rear co-pilot (see Table 3), the transceiver on the right ear and backward oriented (configuration 5) allows the best improvement among the worst gain values for both uplink and downlink.

Tables 12, 13 and 14 show the worst DC gain values for the captain, first officer and rear pilot respectively, with the different transceiver configurations on the headsets from 1 to 5. For each case, best values are highlighted in bold.

For the captain (Table 12), the transceiver on the right ear and backward oriented (configuration 5) leads to the best value for both uplink and downlink.

For the first officer (Table 13), the transceiver on the left ear and backward oriented (configuration 2) leads to the best value for both uplink and downlink. For the rear pilot (Table 14), the transceiver on the right ear and backward oriented (configuration 5) leads to the best values for both uplink and downlink respectively.

We note that in any case, the transceivers with forward orientation on the left ear (configuration 1) and on the right ear (configuration 4), do not bring any improvement, and are not of interest. Therefore, the optimal headset should have only three transceivers respectively located at configurations 2, 3, and 5. Moreover, these best values are different for each crew member. In order to ensure that the performances

TABLE 12. Lowest DC gain (dB) among the transceivers configurations for the captain.

	Uplink	Downlink
Configuration 1, left ear	-70.4	-69.9
Configuration 2, left ear	-70.6	-70.5
Configuration 3, head top	-70.3	-69.7
Configuration 4, right ear	-70.9	-70.1
Configuration 5, right ear	**-66.4**	**-65.6**

TABLE 13. Lowest DC gain (dB) among the transceivers configurations for the first officer.

	Uplink	Downlink
Configuration 1, left ear	-71.1	-70.4
Configuration 2, left ear	**-68.2**	**-67**
Configuration 3, head top	-72.1	-71.2
Configuration 4, right ear	-71.3	-70.7
Configuration 5, right ear	-71.7	-71.6

TABLE 14. Lowest DC gain (dB) among the transceivers configurations for the rear pilot.

	Uplink	Downlink
Configuration 1, left ear	-71.6	-70.8
Configuration 2, left ear	-69.4	-68.5
Configuration 3, head top	-67.9	-68.5
Configuration 4, right ear	-68	-67.5
Configuration 5, right ear	**-66.3**	**-64.7**

are guaranteed for all members, we consider in the analysis the worst gain values among them.

These values corresponding to -68.2 dB in uplink and -67 dB in downlink are both obtained for the transceiver at the co-pilot left ear (configuration 2). These values are the one reported in Table 4.

ACKNOWLEDGMENT

The authors would like to thank the European Union and AIRBUS company for supporting this work through the Cleansky 2 H2020 project titled Aircraft Light Communication (ALC).

REFERENCES

[1] D.-K. Dang, A. Mifdaoui, and T. Gayraud, "Fly-by-wireless for next generation aircraft: Challenges and potential solutions," in *Proc. IFIP Wireless Days*, Dublin, Ireland, 2012, pp. 1–8.

[2] Y. Zou, J. Zhu, X. Wang, and L. Hanzo, "A survey on wireless security: Technical challenges, recent advances, and future trends," *Proc. IEEE*, vol. 104, no. 9, pp. 1727–1765, Sep. 2016.

[3] S. Arnon, J. Barry, G. Karagiannidis, R. Schober, and M. Uysal, *Advanced Optical Wireless Communication Systems*. Cambridge, U.K.: Cambridge Univ. Press, 2012.

[4] S. Arnon, *Visible Light Communication*. Cambridge, U.K.: Cambridge Univ. Press, 2015.

[5] S. Dimitrov and H. Haas, *Principles of LED Light Communications: Towards Networked Li-Fi*. Cambridge, U.K.: Cambridge Univ. Press, 2015.

[6] Z. Ghassemlooy, L. N. Alves, S. Zvanovec, and M.-A. Khalighi, ed., *Visible Light Communications: Theory and Applications*, 1st ed. Boca Raton, FL, USA: CRC Press, 2017.

[7] N. Schmitt, "Wireless optical NLOS communication in aircraft cabin for in-flight entertainment," in *Proc. ESA 1st Opt. Wireless Onboard Commun. Workshop*, Sep. 2004, p. 29.

[8] S. Dimitrov, H. Haas, M. Cappitelli, and M. Olbert, "On the throughput of an OFDM-based cellular optical wireless system for an aircraft cabin," in *Proc. 5th Eur. Conf. Antennas Propag. (EUCAP)*, Rome, Italy, 2011, pp. 3089–3093.

[9] N. Schmitt *et al.*, "Diffuse wireless optical link for aircraft intra-cabin passenger communication," in *Proc. 5th Int. Symp. Commun. Syst. Netw. Digit. Signal Process. CSNDSP*, Jul. 2006, pp. 625–628.

[10] D. Marinos *et al.*, "Medical and safety monitoring system over an in-cabin optical wireless network," *Int. J. Electron.*, vol. 98, no. 2, pp. 223–233, 2011.

[11] S. Dimitrov, R. Mesleh, H. Haas, M. Cappitelli, M. Olbert, and E. Bassow, "Path loss simulation of an infrared optical wireless system for aircrafts," in *Proc. IEEE Global Telecommun. Conf. (GLOBECOM)*, Honolulu, HI, USA, 2009, pp. 1–6.

[12] S. Joumessi-Demeffo *et al.*, "A link reliability study of optical wireless headset inside aircraft cockpit," in *Proc. Global LIFI Congr. (GLC)*, Paris, France, 2019, pp. 1–6.

[13] H. Haas, L. Yin, Y. Wang, and C. Chen, "What is LiFi?" *IEEE J. Lightw. Technol.*, vol. 34, no. 6, pp. 1533–1544, Mar. 15, 2016.

[14] *IEEE Standard for Information Technology—Telecommunications and Information Exchange Between Systems—Local and Metropolitan Networks—Specific Requirements—Part 11: Wireless LAN Medium Access Control (MAC) and Physical Layer (PHY) specifications*, IEEE Standard P802.11bb, 2016.

[15] D. J. F. Barros, S. K. Wilson, and J. M. Kahn, "Comparison of orthogonal frequency-division multiplexing and pulse-amplitude modulation in indoor optical wireless links," *IEEE Trans. Commun.*, vol. 60, no. 1, pp. 153–163, Jan. 2012.

[16] Z. Ghassemlooy, W. Popoola, and S. Rajbhandari, *Optical Wireless Communications: System and Channel Modelling With MATLAB*. Boca Raton, FL, USA: CRC Press, Aug. 2012.

[17] G. A. Mahdiraji and E. Zahedi, "Comparison of selected digital modulation schemes (OOK, PPM and DPIM) for wireless optical communications," in *Proc. 4th Student Conf. Res. Develop.*, Selangor, Malaysia, 2006, pp. 5–10.

[18] A. Behlouli, P. Combeau, L. Aveneau, S. Sahuguede, and A. Julien-Vergonjanne, "Efficient simulation of optical wireless channel application to wbans with MISO link," *Procedia Comput. Sci.*, vol. 40, pp. 190–197, Sep. 2014.

[19] A. Behlouli, P. Combeau, and L. Aveneau, "MCMC methods for realistic indoor wireless optical channels simulation," *IEEE/OSA J. Lightw. Technol.*, vol. 35, no. 9, pp. 1575–1587, May 01, 2017.

[20] (1995). *Blender*. Accessed: Jun. 2020. [Online]. Available: https://www.blender.org

[21] A. Goldsmith, *Wireless Communications*. New York, NY, USA: Cambridge Univ. Press, 2005.

[22] J. M. Kahn and J. R. Barry, "Wireless infrared communications," *Proc. IEEE*, vol. 85, no. 2, pp. 265–298, Feb. 1997.

[23] A. J. C. Moreira, R. T. Valadas, and A. M. de Oliveira Duarte, "Characterisation and modelling of artificial light interference in optical wireless communication systems," in *Proc. 6th Int. Symp. Pers. Indoor Mobile Radio Commun.*, vol. 1. Toronto, ON, Canada, 1995, pp. 326–331.

[24] M. D. Soltani, X. Wu, M. Safari, and H. Haas, "Bidirectional user throughput maximization based on feedback reduction in LiFi networks," *IEEE Trans. Commun.*, vol. 66, no. 7, pp. 3172–3186, Jul. 2018.

[25] G. Bianchi, "Performance analysis of the IEEE 802.11 distributed coordination function," *IEEE J. Sel. Areas Commun.*, vol. 18, no. 3, pp. 535–547, Mar. 2000.

[26] S. Bdulghani, S. Mohd Fadzli, and A. Hasib, "Throughput and delay analysis of IEEE 802.11 DCF in the presence of hidden nodes for multi-hop wireless networks," *Wireless Pers. Commun.*, vol. 79, pp. 907–927, Nov. 2014.

[27] R. Khalili and K. Salamatian, "A new analytic approach to evaluation of packet error rate in wireless networks," in *Proc. 3rd Annu. Commun. Netw. Serv. Res. Conf. (CNSR'05)*, Halifax, NS, Canada, 2005, pp. 333–338.

[28] *Safety of Laser Products—Part 1. Equipment Classification and Requirement*, Standard IEC 60825-1.2007, 2007. [Online]. Available: https://www.iecee.org/dyn/www/f?p=106:49:0::::FSP_STD_ID:3587

[29] *Photobiological Safety of Lamps and Lamp Systems*, Standard IEC 62471.2006, 2006. [Online]. Available: https://www.iecee.org/dyn/www/f?p=106:49:0::::FSP_STD_ID:7076

[30] *Radio Technical Commission for Aeronautics DO-214/SC-164. 214: Audio Systems Characteristics and Minimum Operational Performance Standards for Aircraft Audio Systems and Equipment Systems and Equipment*, RTCA, Washington, DC, USA, 1993.
[31] P. Combeau *et al.*, "Optical wireless channel simulation for communications inside aircraft cockpits," *IEEE/OSA J. Lightw. Technol.*, early access, Jun. 22, 2020, doi: 10.1109/JLT.2020.3003989.

STEVE JOUMESSI-DEMEFFO received the undergraduation degree in telecommunications from the University of Poitiers in 2015, and the M.Sc. degree in informatics from the University of Nantes in 2016. He is currently pursuing the Ph.D. degree with the University of Limoges, France, where his researches are developed within the XLIM Laboratory (UMR CNRS 7252) and concern implementation of optical wireless networks, precisely for aircraft use case.

STÉPHANIE SAHUGUÈDE received the M.Sc. and M.Eng. degrees from the National School of Engineers of Limoges (ENSIL-ENSCI), University of Limoges, France, in 2006, and the Ph.D. degree in high frequencies and optical telecommunications from the University of Limoges in 2009, where she is currently works as an Associate Professor with XLIM Laboratory (UMR CNRS 7252) and ENSIL-ENSCI. Her research activities include error correction codes, optical CDMA, wireless optical communications, and communication systems for e-Health.

ANNE JULIEN-VERGONJANNE received the Ph.D. degree in microwave and optical communications from the University of Limoges, France, in 1987. Since 2006, she has been a Professor with the National School of Engineers (ENSIL-ENSCI), Limoges, and develops research activities within the XLIM Laboratory, UMR CNRS 7252, University of Limoges. She leads the SYCOMOR Research Team, SRI Axis (Systems and Intelligent Networks), around optical and radio communication systems and networks. Her current research activities are in the fields of optical wireless communication systems. She is the XLIM Scientific Leader for European project H2020 Cleansky2 Aircraft Light Communication. She is a member of IEEE Communication Society.

PIERRE COMBEAU received the Ph.D. degree in signal processing and telecommunications from the University of Poitiers, France, in 2004. Since 2005, he has been an Associate Professor with the XLIM Laboratory, UMR CNRS 7252, University of Poitiers, France. His current research includes the study of the electromagnetic waves propagation for wireless communication systems in radio and optical frequency domains.